Particle-in-cell simulations of collisionless magnetic reconnection with a non-uniform guide field

F. Wilson, T. Neukirch, M. Hesse, M. G. Harrison, and C. R. Stark

Citation: Physics of Plasmas **23**, 032302 (2016); doi: 10.1063/1.4942939
View online: http://dx.doi.org/10.1063/1.4942939
View Table of Contents: http://scitation.aip.org/content/aip/journal/pop/23/3?ver=pdfcov
Published by the AIP Publishing

Particle-in-cell simulations of collisionless magnetic reconnection with a non-uniform guide field

F. Wilson,[1,a)] T. Neukirch,[1,b)] M. Hesse,[2] M. G. Harrison,[1] and C. R. Stark[1,3]
[1]School of Mathematics and Statistics, University of St Andrews, St Andrews KY16 9SS, United Kingdom
[2]NASA Goddard Space Flight Center, Greenbelt, Maryland 20771, USA
[3]Division of Computing and Mathematics, Abertay University, Dundee DD1 1HG, United Kingdom

(Received 24 December 2015; accepted 12 February 2016; published online 2 March 2016)

Results are presented of a first study of collisionless magnetic reconnection starting from a recently found exact nonlinear force-free Vlasov–Maxwell equilibrium. The initial state has a Harris sheet magnetic field profile in one direction and a non-uniform guide field in a second direction, resulting in a spatially constant magnetic field strength as well as a constant initial plasma density and plasma pressure. It is found that the reconnection process initially resembles guide field reconnection, but that a gradual transition to anti-parallel reconnection happens as the system evolves. The time evolution of a number of plasma parameters is investigated, and the results are compared with simulations starting from a Harris sheet equilibrium and a Harris sheet plus constant guide field equilibrium.
[http://dx.doi.org/10.1063/1.4942939]

I. INTRODUCTION

Magnetic reconnection is one of the most fundamental plasma processes and plays an important role in the magnetic activity of many astrophysical and laboratory plasmas.[1,2] It allows the conversion of stored magnetic energy into bulk flow, thermal, and non-thermal energy, through changes in magnetic connectivity. In many astrophysical plasmas, the effects of particle collisions are negligible, and various aspects of collisionless reconnection have previously been studied in great detail.[3–24] One particular aspect which has been investigated by a number of authors (e.g., Refs. 8, 10–17,19, and 21) is the influence of a guide field on the reconnection process. Most of these studies have used a Harris sheet[25] with a constant guide field as an initial current sheet configuration.

The addition of a constant guide field to the Harris sheet affects the evolution in a number of ways (see e.g., Ref. 2 for a more comprehensive overview than what we describe here). Some important points to note are as follows:

(a) A constant guide field (of sufficient magnitude) has been shown to reduce the reconnection rate.[8,12,13]
(b) The structure of the diffusion region is changed with the addition of a constant guide field.[2] In the anti-parallel (Harris sheet) case, the different outflow trajectories of the ions and electrons generate in-plane current loops (Hall currents), which in turn generate a quadrupolar out-of-plane magnetic field.[4,9] The addition of a constant (out-of-plane) guide field results in a distortion of this quadrupolar field.[8,10] Furthermore, there is a strong parallel component to the out-of-plane electric field, which generates strong out-of-plane currents, and in-plane components of the parallel electron flows produce a density asymmetry along the separatrices.
(c) As a result of the density asymmetry described in point (b), in guide field reconnection, there is a rotation of the reconnecting current sheet(s).[10,12,14,15,17,21]
(d) A guide field affects the particle orbits in the electron diffusion region[21]—it can destroy the bounce motion which occurs across the field reversal in the anti-parallel case, and so the length scales characterizing the orbits in each case are different. In the guide field case, the relevant scale is the electron Larmor radius in the guide field, whereas in the anti-parallel case, it is the electron bounce width in the reconnecting field component.
(e) A consequence of point (d) is that the addition of a guide field leads to thinner current sheets than in the anti-parallel case.[17]

In this paper, we wish to address the following question: does the reconnection process change (and, if so, how?) if we use an initial current sheet configuration with a non-uniform guide field? We present results of a 2.5D particle-in-cell (PIC) simulation, in which we use an exact self-consistent equilibrium for the force-free Harris sheet as an initial condition.[26,27]

Since the equilibrium guide field of the force-free Harris sheet (here $B_y = B_0/\cosh(z/L)$) decreases with distance from the centre of the current sheet, we expect that the system will initially show features of guide field reconnection, but that a gradual transition to anti-parallel reconnection should take place, because plasma with smaller guide field strength should be transported towards the reconnection region as the system evolves in time. We will investigate whether and how this transition takes place, and also how it is reflected in the time evolution of plasma quantities

a)Electronic Mail: fw237@st-andrews.ac.uk
b)Electronic Mail: tn3@st-andrews.ac.uk

relevant for collisionless reconnection, such as the off-diagonal, non-gyrotropic elements of the electron pressure tensor.

Three-dimensional PIC simulations have previously been carried out for a magnetic field profile similar to that of the force-free Harris sheet,[15] but with an additional constant guide field added in the same direction as the non-uniform guide field. The initial particle distribution functions were taken to be drifting Maxwellian distributions, which do not represent an exact initial equilibrium for this configuration. This leads us to discuss another motivation for our work—we are not aware of any previous study of collisionless reconnection for which exactly force-free initial conditions have been used for a nonlinear force-free field. The only known studies to use exactly force-free initial conditions have started from a linear force-free configuration.[28–32] Exact collisionless equilibria for such 1D linear force-free fields were first found approximately five decades ago,[33,34] but the first exact equilibria of this type for nonlinear force-free fields were found only very recently.[26,27,35–38] Hence, only preliminary investigations have been carried out into the linear and nonlinear collisionless stability and dynamics of these configurations.[39,40]

The structure of the paper is as follows. In Sec. II, we discuss the simulation setup, followed by a detailed description of the results in Sec. III. We conclude with a summary and conclusions in Sec. IV.

II. SIMULATION SETUP

A. Overview of initial configuration

For the main simulation run to be discussed, the initial magnetic field configuration is a force-free Harris sheet with added perturbation $\mathbf{B}_p = B_{xp}\hat{\mathbf{x}} + B_{zp}\hat{\mathbf{z}}$

$$\mathbf{B} = B_0(\tanh(z/L) + B_{xp}, 1/\cosh(z/L), B_{zp}), \tag{1}$$

where L is the current sheet half-width. The perturbation components have the form

$$B_{xp} = -a_0 x_m \frac{\pi}{2L_z}\exp\left(-\frac{x^2}{2x_m^2} + 0.5\right)\sin\left(\frac{\pi z}{2L_z}\right)$$
$$B_{zp} = a_0 \frac{x}{x_m}\exp\left(-\frac{x^2}{2x_m^2} + 0.5\right)\cos\left(\frac{\pi z}{2L_z}\right), \tag{2}$$

where L_z is the half-width of the numerical box in the z-direction, $a_0 = 0.1$ and $x_m = L_z/2$. This gives an X-point reconnection site at the centre of the numerical box and allows the nonlinear phase of the evolution to be studied without considering the cause of the reconnection onset.

The x-component of the force-free Harris sheet magnetic field (when $\mathbf{B}_p = 0$) has the same spatial structure as that of the Harris sheet,[25] and there is a non-uniform guide field in the y-direction, which is chosen in such a way that the total magnetic field strength is spatially uniform, and is given by $B_0^2 = B_x^2 + B_y^2$. The resulting current density is parallel to the magnetic field, and hence, the equilibrium is force-free.[26,27] A further consequence is that both the plasma density and P_{zz}, the component of the pressure tensor that keeps the equilibrium in force balance, are spatially uniform. The equilibrium also has non-zero current density components in both the x- and y-directions, given by

$$\mathbf{j} = \frac{B_0}{\mu_0 L}\frac{1}{\cosh^2(z/L)}\left(\sinh(z/L)\hat{\mathbf{x}} + \hat{\mathbf{y}}\right). \tag{3}$$

To initialise the particle positions and velocities in our main simulation run, we use the distribution function[26,27]

$$f_s = f_{0s}\exp(-\beta_s H_s) \times[\exp(\beta_s u_{ys} p_{ys}) + a_s\cos(\beta_s u_{xs} p_{xs}) + b_s], \tag{4}$$

where $H_s = (m_s/2)(v_x^2 + v_y^2 + v_z^2)$ is the particle energy, and $p_{xs} = m_s v_s + q_s A_x$ and $p_{ys} = m_s v_y + q_s A_y$ are the x- and y-components of the canonical momentum (for mass m_s, charge q_s, and vector potential components $A_x = 2B_0 L\arctan(e^{z/L})$ and $A_y = -B_0 L\ln[\cosh(z/L)]$). The parameter β_s is defined as $\beta_s = (k_B T_s)^{-1}$, where T_s is the constant temperature of species s. Additionally, f_{0s}, a_s, b_s, u_{xs}, and u_{ys} are constant parameters.

The distribution function (4) consists of a part which is equal to the Harris sheet distribution function,[25] and an extra part which arises from the non-uniform guide field of the force-free Harris sheet. It should be noted that it can have a non-Maxwellian structure in velocity space. For further details of the properties of this function, see Refs. 26 and 27.

To analyse the expected transition from guide field to anti-parallel reconnection in the force-free Harris sheet case, we will also present results from two other simulation runs: one which starts from a Harris sheet, and the other from a Harris sheet plus uniform guide field of $B_y = B_0$.

B. Normalisation and parameters

To study the reconnection process, we use a 2.5D fully electromagnetic particle-in-cell code, which has been frequently used by Hesse and co-authors (see, for example, Refs. 5 and 9). The normalisation is as follows: the magnetic field is normalised to B_0; the number density to a free parameter, n_0; times to $\Omega_i^{-1} = (eB_0/m_i)^{-1}$ (the inverse of the ion cyclotron frequency in the equilibrium magnetic field); and lengths to the ion inertial length, c/ω_i, where $\omega_i = (e^2 n_0/\epsilon_0 m_i)^{1/2}$ is the ion plasma frequency. Furthermore, velocities are normalised to the ion Alfvén velocity, $v_A = \sqrt{\mu_0 m_i n_0}$, and so current densities and electric fields are normalised to $B_0/(\mu_0 c/\omega_i)$ and $v_A B_0$, respectively.

In all simulation runs, we use an ion-electron mass ratio of $m_i/m_e = 25$. The total number of particles is 1.44×10^9. The grid spacing in x and z is $n_x = 1200$, $n_z = 600$, and hence, there are 2000 particles per cell. The numerical box has length $L_x = 64.0$ and width $L_z = 32.0$, which gives a grid spacing of $\Delta x = \Delta z = 0.053$. The boundary conditions are periodic at the x-boundaries, and specularly reflecting at the z-boundaries. The time step chosen is $dt = 0.5/\omega_e$ (where ω_e is the electron plasma frequency), with smaller time steps used occasionally. The ratio ω_e/Ω_e is set to equal 5. The ion-electron temperature ratio is equal to unity, with

$T_i + T_e = 0.5$, so that $T_i = T_e = 0.25$. The current sheet half-thickness is equal to one ion inertial length: $L = 1.0$.

The various parameters from the force-free Harris sheet distribution function (4) have the following values: $u_{xe}/v_{th,e} = u_{ye}/v_{th,e} = \pm 0.2$, $u_{xi}/v_{th,i} = u_{yi}/v_{th,i} = \pm 1.0$, $a_e = 0.52$, $a_i = 1.36$, $b_e = 1.02$, and $b_i = 1.65$. Using conditions derived in Ref. 27, it can be seen that this combination of parameters corresponds to a case where the ion distribution function is single-peaked in both v_y and v_z, but has a double maximum in the v_x-direction, for small values of z around zero. The electron distribution function is single-peaked in all three velocity components.

III. RESULTS

A. Evolution of magnetic field and current density

Figure 1 shows the time evolution of the reconnected flux for the three simulation runs, and reconnection rates are shown in Figure 2. The maximum reconnection rate is highest in the Harris sheet case, occurring at $t = 18$. It has been observed in the previous work that the effect of a constant guide field (of significant magnitude) is to reduce the maximum reconnection rate.[8,12,13] We see here that in the force-free run, the maximum reconnection rate is further reduced from that of the constant guide field. It should be noted, however, that we used a parameter combination such that the initial electron number density is 25% higher in the force-free case than in the other two cases, which will have an effect on the reconnection rate.

Figure 3 shows the y-component of the current density (in colour) and the projection of the magnetic field lines on to the x-z-plane, at various times for the force-free run. The figures show how reconnection leads to global changes in the structure of both quantities. At $t = 0$, it can be seen that the perturbation (2) to the magnetic field gives an initial X-point in the centre of the box. As time proceeds initially, a strong current sheet develops in the central region, and is slightly inclined, which is a typical feature of guide field reconnection.[21] As time proceeds beyond $t = 20$, the current sheet becomes more aligned with the x-axis, which could be a sign of a transition from guide field to anti-parallel reconnection.

Looking closely at Figure 3 for $t = 20$, it can be seen that a small magnetic island has started to form, which is a result of

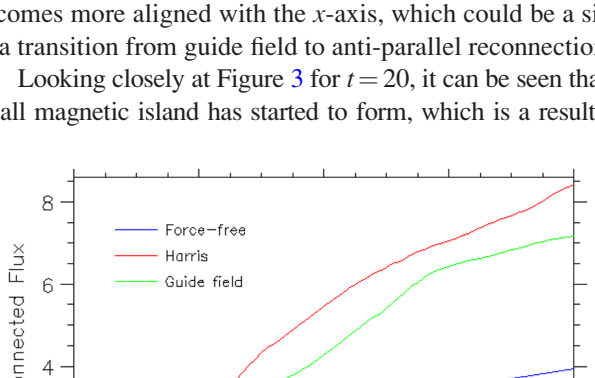

FIG. 1. Reconnected flux for each simulation run.

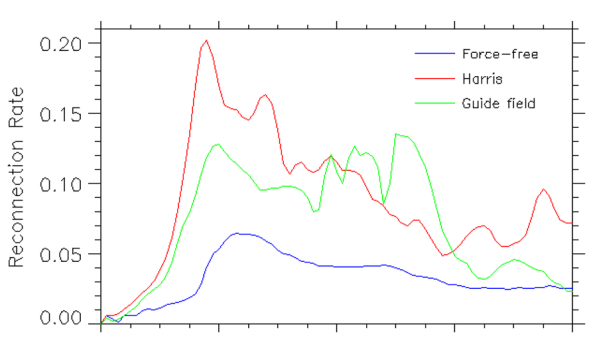

FIG. 2. Reconnection rate for each simulation run.

the bifurcation of the original X-point reconnection site into two new reconnection regions[9]—one to the left of the island and one to the right, which can be seen more clearly at later times. This is a feature commonly seen in reconnection simulations. Beyond $t = 20$, the island proceeds to move to the left, and eventually disappears, as the right-hand X-point begins to dominate over the left-hand one. By the end of the simulation, at $t = 80$, the island is no longer visible, and there is only one remaining reconnection region, which has shifted back towards the centre of the box. There is still a relatively strong current in this region though, which is higher than the original j_y.

Figure 4 shows the evolution of the non-uniform guide field in the force-free case. It can again be seen how the magnetic island starts to form around $t = 20$, and eventually disappears. At $t = 40$ and at subsequent times, a modified quadrupolar structure of B_y can be seen around the X-point. This structure is qualitatively similar to that seen in Harris plus constant guide field simulations,[8,10] and so we do not see a transition to the quadrupolar structure seen in Harris sheet simulations.[4,8,9] Figure 5 shows the variation of B_y at the dominant X-point with time. It can be seen that, on the whole, there is a downward trend as time proceeds, representing a gradual transition from guide field to anti-parallel reconnection (where B_y would be close to zero). From around $t = 35$ onwards, B_y fluctuates around a value of approximately 0.15. Of course, we do not have totally anti-parallel reconnection by the end of the simulation, but B_y has clearly been significantly decreased from its initial value of 1.0 at the X-point.

Figure 6 shows the x-component of the current density in the force-free case. The equilibrium j_x is anti-symmetric (see Eq. (3)). As time proceeds, there is a build up of j_x in the magnetic islands. These regions of strong j_x correspond to regions where there is a strong gradient in the y-component of the magnetic field (see Figure 4). Similar behaviour has been seen in linear force-free simulations, and also in preliminary force-free Harris sheet simulations.[39] We have not included similar plots for the Harris and Harris plus constant guide field runs, but comment that j_x is more prominent in the force-free case, which is to be expected since the other two cases have zero equilibrium j_x.

B. Electron Larmor radius and bounce width

In order to further investigate the expected transition from guide field to anti-parallel reconnection, we now

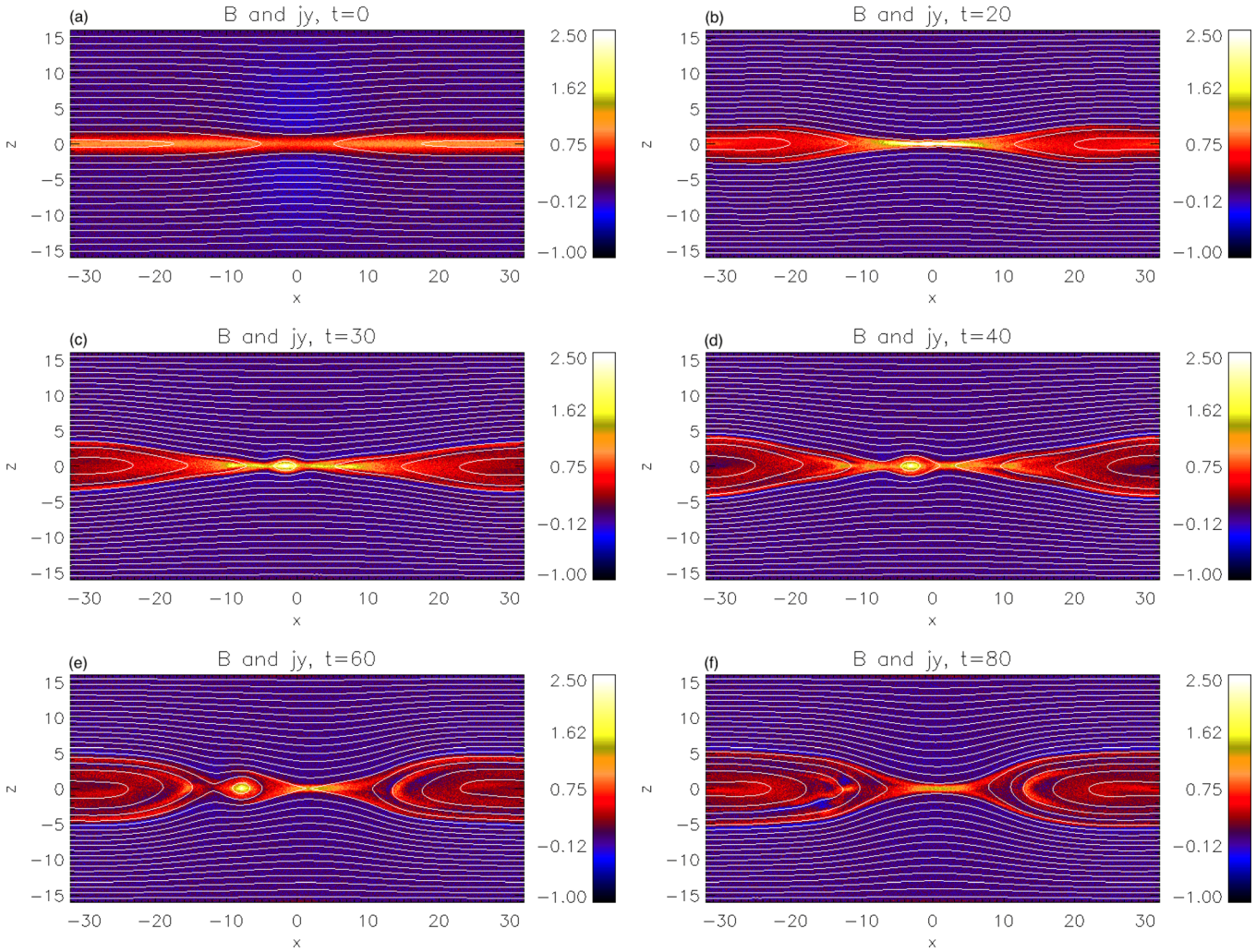

FIG. 3. Evolution of j_y and the magnetic field lines for the force-free run at (a) $t = 0$, (b) $t = 20$, (c) $t = 30$, (d) $t = 40$, (e) $t = 60$, (f) $t = 80$.

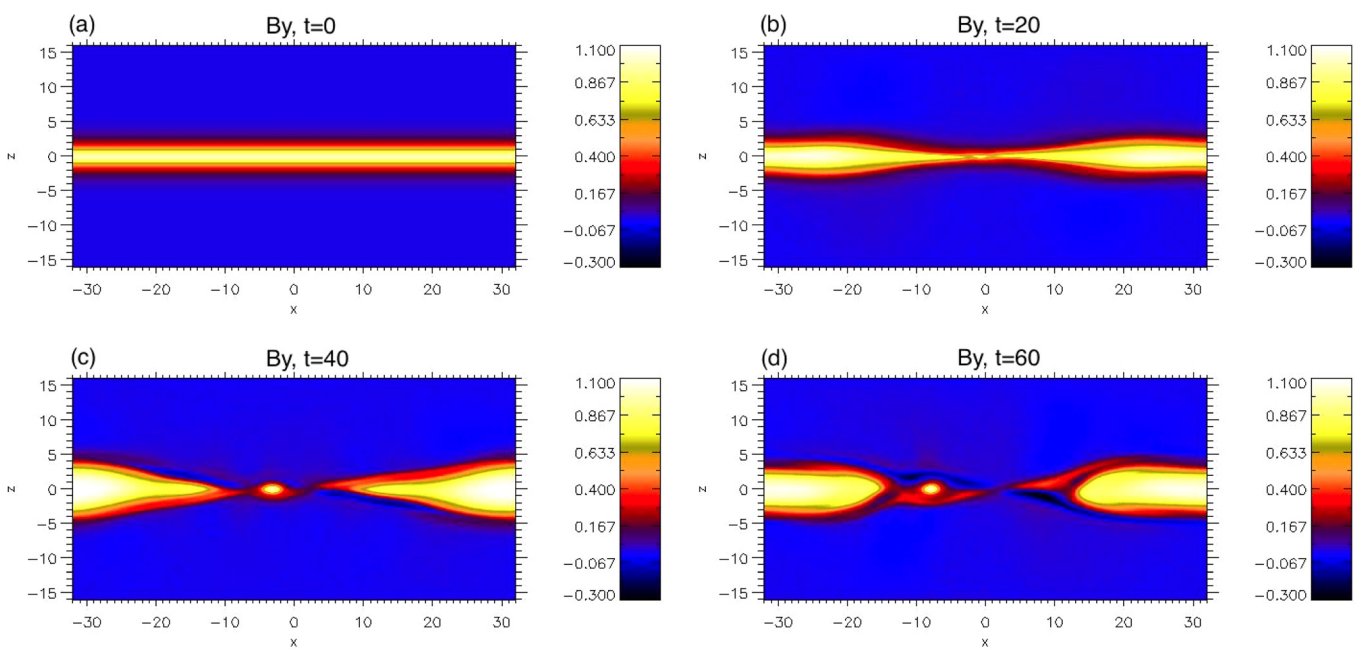

FIG. 4. Evolution of B_y in the force-free case at (a) $t = 0$, (b) $t = 20$, (c) $t = 40$, (d) $t = 60$.

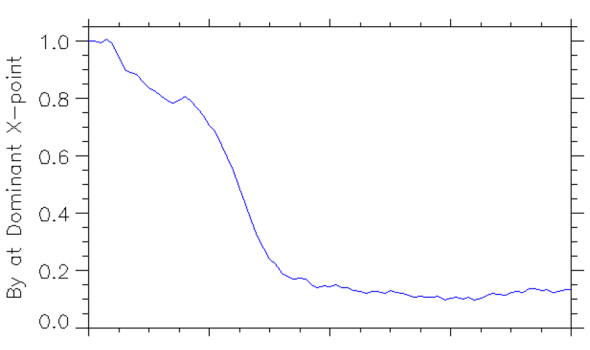

FIG. 5. B_y at the dominant X-point, as a function of time.

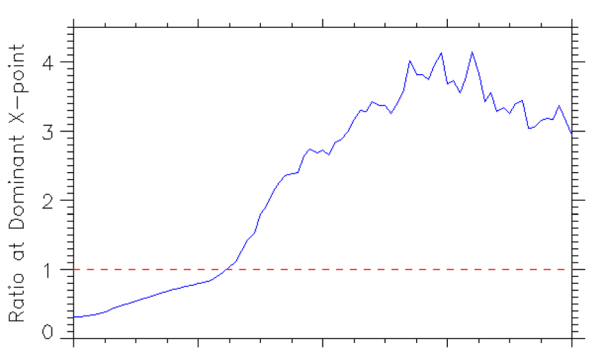

FIG. 7. Ratio of the electron Larmor radius in the guide field B_y and the electron bounce width, λ_z, plotted against time. A horizontal line is plotted at $r_{Ley}/\lambda_z = 1$.

consider the relevant length scales for the reconnection electric field. In the case of a guide field of significant magnitude, the electrons are strongly magnetised in the electron diffusion region, and $r_{Ley} = v_{th,e}/(eB_y/m_e)$, the thermal electron Larmor radius in the guide field B_y is the characteristic length scale.[21] As the guide field gets weaker, however, the important scale length is the electron bounce width in the reconnecting field component B_x, given by

$$\lambda_z = \left(\frac{2m_e k_B T_e}{e^2(\partial B_x/\partial z)^2}\right)^{1/4}. \tag{5}$$

As discussed in Ref. 21, the effect of the guide field B_y on the electron orbits is significant if

$$r_{Ley} \leq \lambda_z. \tag{6}$$

When the condition (6) is satisfied at the reconnection site, therefore, we would expect to see mainly signatures of guide field reconnection, and when it is no longer satisfied, we would expect that this has coincided with a gradual transition towards anti-parallel reconnection and would expect to see some signatures of this.

In Figure 7, the ratio r_{Ley}/λ_z is plotted as a function of time. It first goes above unity between $t = 24$ and $t = 25$. We will consider $t = 25$ to be the "transition time" towards anti-parallel reconnection, since after this time, the ratio ceases to fluctuate around unity. Figure 8 shows the y-component of the current density and the magnetic field lines at this time (for the force-free run), together with plots at $t = 18$ and $t = 16$ for the Harris plus constant guide field and Harris runs, respectively, (these are the times at which the reconnected flux in both cases matches that of the force-free case at $t = 25$). On the macroscopic level, the field-line structure looks more like that from the Harris sheet case, with an island separating two X-points. The central current sheet in the force-free case is still slightly inclined, but not as much as seen in Figure 3 at $t = 20$, and this inclination is also not as strong as seen in the constant guide field case.

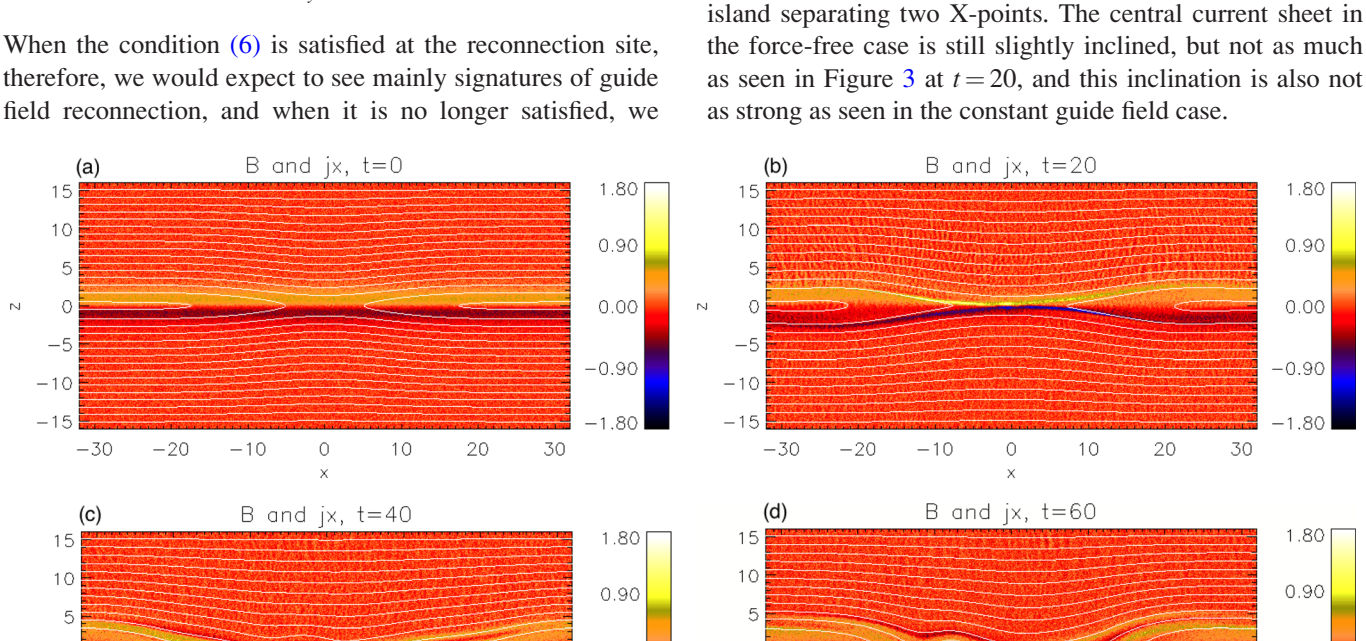

FIG. 6. Evolution of j_x and the magnetic field lines for the force-free run at (a) $t = 0$, (b) $t = 20$, (c) $t = 40$, (d) $t = 60$.

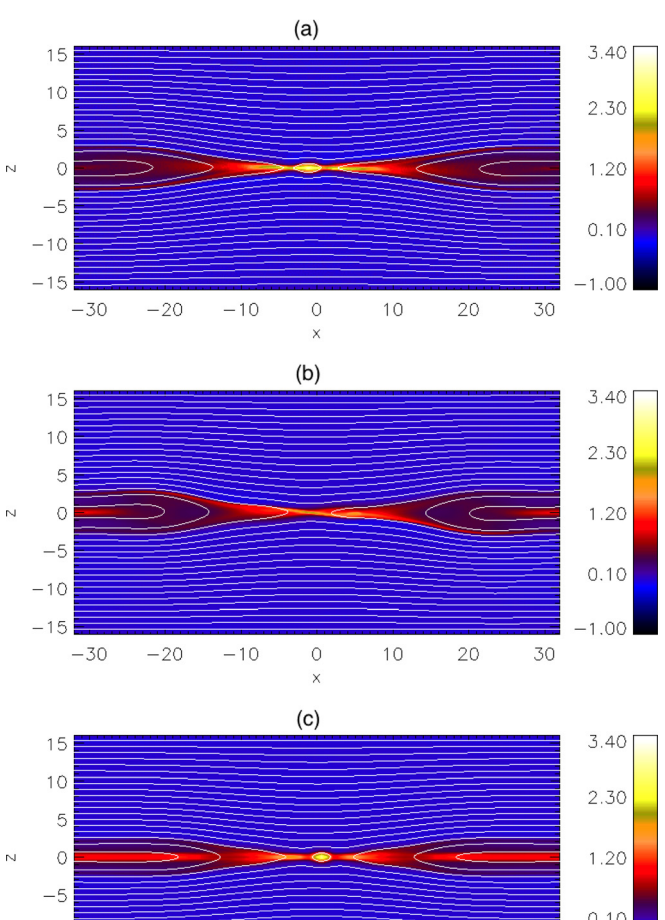

FIG. 8. Evolution of j_y and the magnetic field lines, for (a) the force-free case at the "time of transition" to anti-parallel reconnection (t = 25), and the corresponding times at which the reconnected flux is the same in (b) the constant guide field case (t = 18) and (c) the Harris case (t = 16).

C. The reconnection electric field

In a 2D setup, the reconnection electric field is given by

$$E_y = (v_{xe}B_z - v_{ze}B_x) - \frac{1}{en_e}\left(\frac{\partial P_{xye}}{\partial x} + \frac{\partial P_{yze}}{\partial z}\right) - \frac{m_e}{e}\left(\frac{\partial v_{ye}}{\partial t} + v_{ex}\frac{\partial v_{ey}}{\partial x} + v_{ez}\frac{\partial v_{ey}}{\partial z}\right), \quad (7)$$

where the first bracket represents convection, the second represents the effect of the off-diagonal pressure tensor components, and the last bracket represents the effect of bulk inertia.

Figures 9 and 10 show, for the force-free case, the contributions from each of the terms on the right-hand side of Eq. (7) to the reconnection electric field, along x and z, through the average position of the dominant X-point, for data averaged between $t = 24$ and $t = 26$. The time we chose to average around is the "transition time" discussed in Section III B, where the dominant scale for the evolution switches from the Larmor radius in the guide field B_y to the electron bounce width λ_z. The pressure gradient terms are

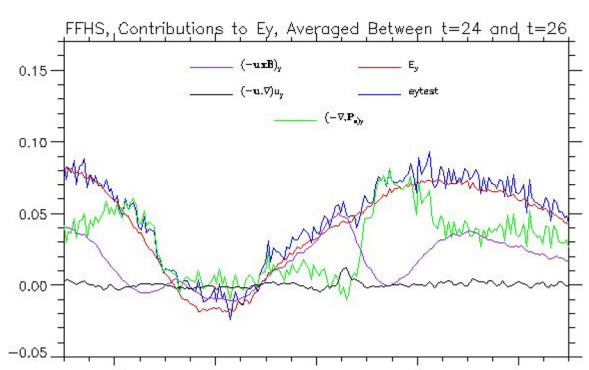

FIG. 9. Contributions to E_y along x, through the dominant X-point, for data averaged around the transition point at $t = 25$.

graphed as green lines, the convection term as purple lines, and the inertial term as black lines. The sum of these three terms, referred to as "eytest," is plotted as a blue line in both plots. Although this fluctuates due to random noise, it can be seen that in both plots, it matches reasonably well with the E_y that is calculated on the numerical grid in the code (indicated by red lines).

From Figure 9, it can be seen that the pressure gradient term in x is significantly enhanced around the dominant X-point ($x = 1.39$). This increase in pressure coincides with a decrease (towards zero) of the convection term. Such behaviour can also be seen at $x \approx -3.75$, which corresponds roughly to the position of the second, less dominant X-point (see Figure 8). In comparison with the other terms, the inertial term is small. The convection term should of course vanish at any X-points, since they are stagnation points where $\mathbf{v}_s = 0$, and so the pressure gradient term acts to support the reconnection electric field. This is in agreement with what has been found previously for Harris sheet and Harris sheet plus constant guide field simulations.[3,5–8,12,13,16]

From Figure 10, it can be seen that, at $z = 0$ (the position of the dominant X-point), the convection term drops to zero, and again the main contribution to E_y comes from the pressure term. The inertial term is virtually zero everywhere, apart from in the small region surrounding the X-point.

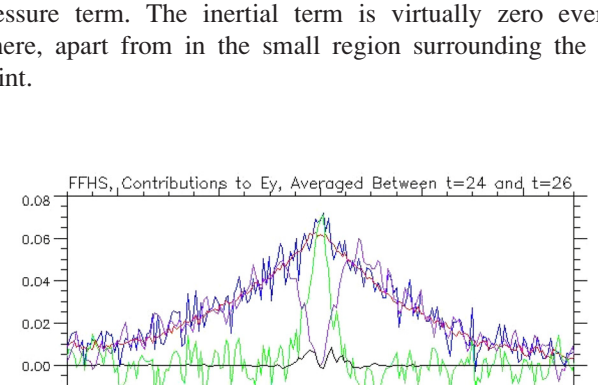

FIG. 10. Contributions to E_y along z, through the dominant X-point, for data averaged around the transition point at $t = 25$.

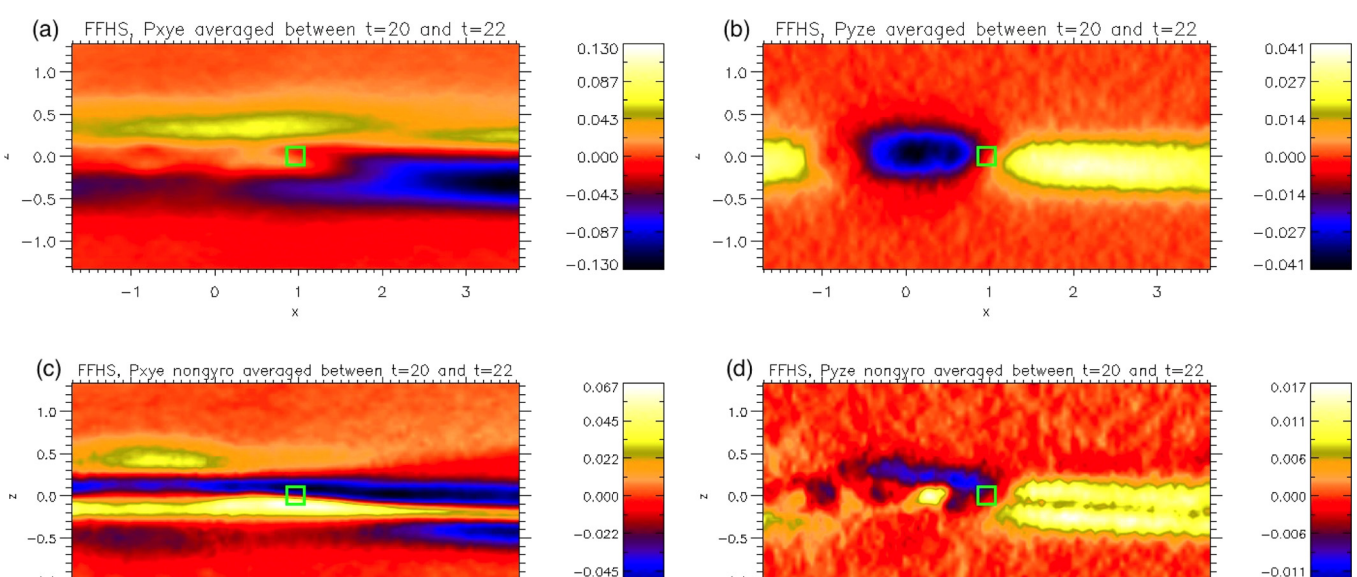

FIG. 11. Electron pressure tensor components for the force-free case, for data averaged between $t = 20$ and $t = 22$. Shown are (a) P_{xye}, (b) P_{yze}, (c) $P_{xye,ng}$, (d) $P_{yze,ng}$.

D. Pressure tensor components

We now focus on the structure of the off-diagonal components of the electron pressure tensor in the diffusion region, restricting attention to the electron quantities, since they are the dominant current carriers. Of particular importance are the non-gyrotropic components, which are given by[21]

$$\underline{\mathbf{P}}_{e,ng} = \underline{\mathbf{P}}_{e} - \underline{\mathbf{P}}_{e,g}, \tag{8}$$

where

$$\underline{\mathbf{P}}_{e,g} = p_{\perp}\underline{\mathbf{I}} + \frac{p_{\parallel} - p_{\perp}}{B^2}\mathbf{BB}, \tag{9}$$

is the gyrotropic component. The term $(\nabla \cdot \underline{\mathbf{P}}_{e,g})_y$ vanishes at any X-points, since B_x and B_z vanish, and so non-gyrotropies of the pressure are required to give a contribution to the reconnection electric field.[12]

Figures 11 to 13 show plots of the xy- and yz-components of the electron pressure tensor, together with the corresponding non-gyrotropic parts, at an early stage of the evolution, at which the total reconnected flux is the same in each case. The data have been averaged between $t = 20$ and $t = 22$ for the force-free run, $t = 12$ and $t = 14$ for the Harris run, and $t = 13.87$ and $t = 15.87$ for the constant guide field run. Note that we only show the non-gyrotropic components in the Harris case (Figure 12), because they are almost identical to the plots of the total P_{xye} and P_{yze}. The average location of the X-point under consideration is indicated by a green square. From Figure 11 for the force-free case, it can be seen that both P_{xye} and $P_{xye,ng}$ have a gradient primarily in z, which is comparable to that from the constant guide field case in Figure 13. The structure of P_{yze} and $P_{yze,ng}$ are also comparable to that from the constant guide field case in the vicinity of the X-point—these components all have gradients in x. Note, however, that $P_{yze,ng}$ in the constant guide field case also has a significant gradient in z, and so there is a significant difference in this component between the force-free and constant guide field cases. The structure of all pressure components in the vicinity of the X-point for the force-free case differs considerably from that of the Harris sheet case, which clearly has horizontal gradients in P_{xye} and vertical gradients in P_{yze}. It can be said, therefore, that in the early stages of the evolution, the pressure in the force-free case exhibits (qualitatively) more features of guide field reconnection than anti-parallel reconnection.

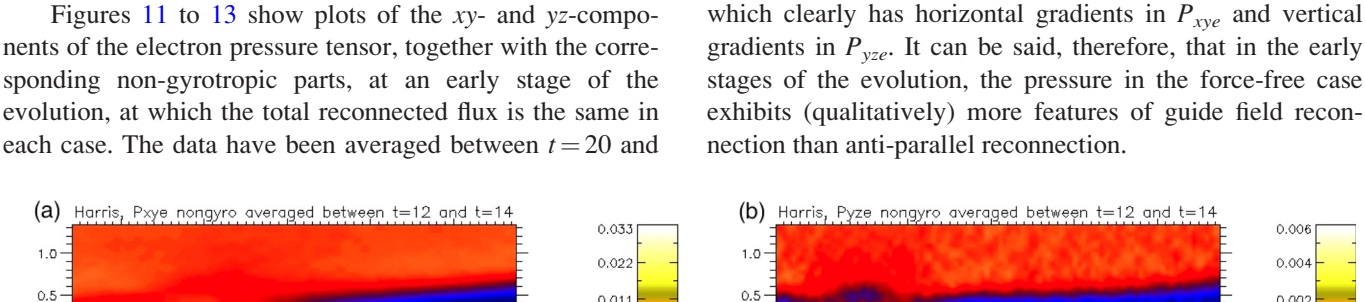

FIG. 12. Electron pressure tensor components for the Harris case, for data averaged between $t = 12$ and $t = 14$. Shown are (a) $P_{xye,ng}$ and (b) $P_{yze,ng}$.

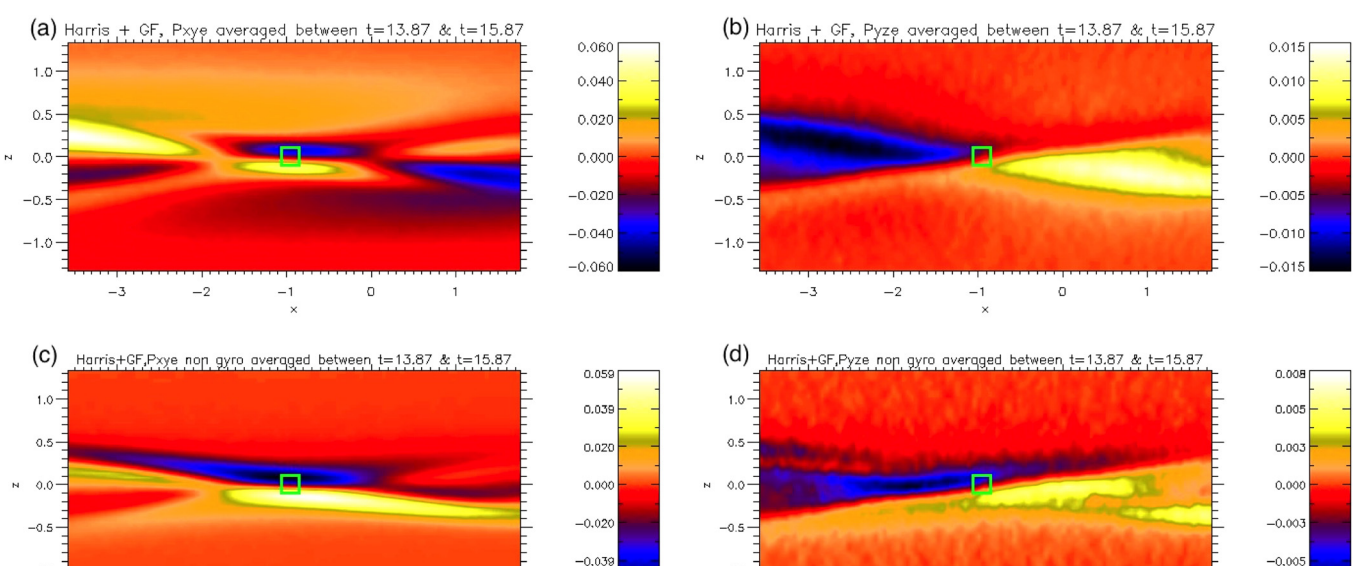

FIG. 13. Electron pressure tensor components for the constant guide field case, for data averaged between $t = 13.88$ and $t = 15.88$. Shown are (a) P_{xye}, (b) P_{yze}, (c) $P_{xye,ng}$, (d) $P_{yze,ng}$.

As we discussed in Section III B, there is a change in the important scale length for the evolution around $t = 25$, from the Larmor radius in the guide field B_y to the electron bounce width λ_z. Figure 14 shows non-gyrotropic pressure plots for the force-free case, for data averaged around this transition time (between $t = 24$ and $t = 26$). On the whole, in the vicinity of the X-point, the structures remain qualitatively more similar to those from the constant guide field case (Figure 13) than the Harris case (Figure 12).

To further investigate the transition, therefore, we now focus on a later time in the evolution. Figures 15–17 show the pressure components for data averaged between $t = 45$ and $t = 47$ for the force-free case, $t = 25$ and $t = 27$ for the constant guide field case, and $t = 20$ and $t = 22$ for the Harris case. As with the earlier Harris plot (Figure 12), we only show the non-gyrotropic components in Figure 16, because again they are almost identical to the plots of the total P_{xye} and P_{yze}. The structure of both P_{xye} and $P_{xye,ng}$ in the force-free case is now significantly different than at earlier times. Focusing on the non-gyrotropic component, $P_{xye,ng}$, the gradient is now primarily in the horizontal direction and looks comparable (qualitatively) to $P_{xye,ng}$ for the Harris sheet. The other non-gyrotropic component, $P_{yze,ng}$, now has significant gradients in both x and z, and still looks more similar to P_{yze} in the guide field case than in the Harris sheet case. From Figures 15–17, we can conclude that some sort of transition has taken place in the structure of the pressure, since we see some signatures of anti-parallel reconnection. We can also conclude from this that the transition is not as simple as being from purely guide field reconnection to purely anti-parallel reconnection, but instead, we see initially primarily signatures of guide field reconnection and signatures of both guide field and anti-parallel reconnection as the system evolves. This may be due to the fact that while B_y at the dominant reconnection site (see Figure 5) decreases over time, it does not actually vanish completely, and Figure 4 shows that there is a modified quadrupolar structure of B_y at later times—so not a transition to the quadrupolar structure seen in Harris sheet simulations. We speculate that this could cause some features of guide field reconnection to persist.

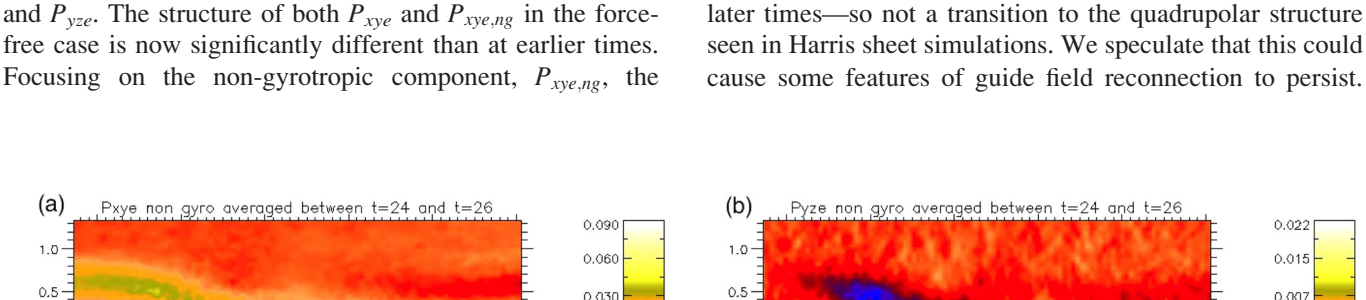

FIG. 14. Electron pressure tensor components for the force-free case, for data averaged between $t = 24$ and $t = 26$ (around the "transition time" at $t = 25$). Shown are (a) $P_{xye,ng}$, (b) $P_{yze,ng}$.

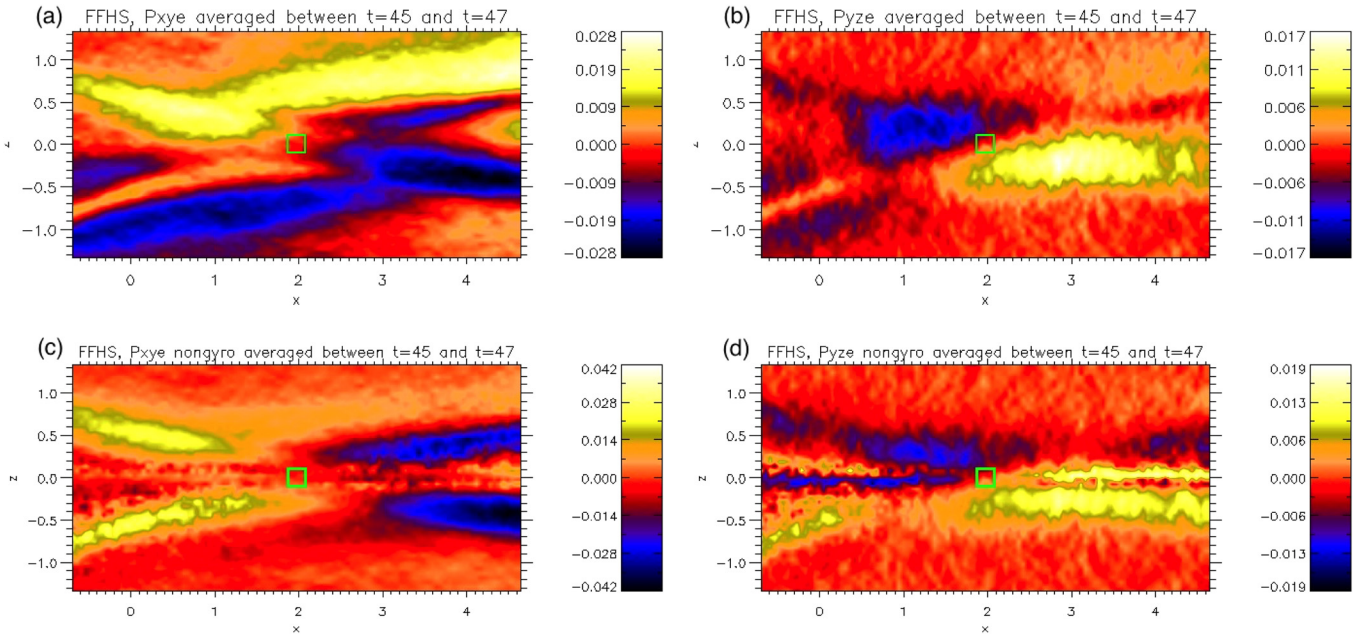

FIG. 15. Electron pressure tensor components for the force-free case, for data averaged between $t = 45$ and $t = 47$. Shown are (a) P_{xye}, (b) P_{yze}, (c) $P_{xye,ng}$, (d) $P_{yze,ng}$.

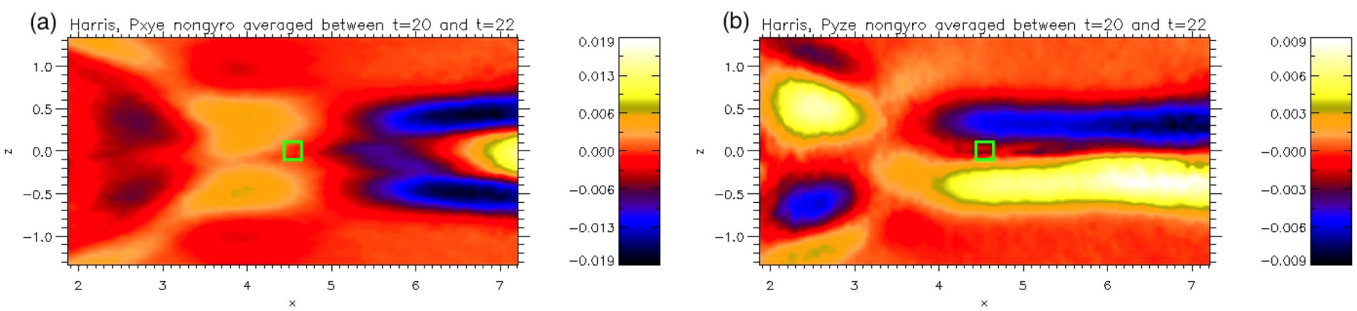

FIG. 16. Electron pressure tensor components for the Harris case, for data averaged between $t = 25$ and $t = 27$. Shown are (a) $P_{xye,ng}$, (b) $P_{yze,ng}$.

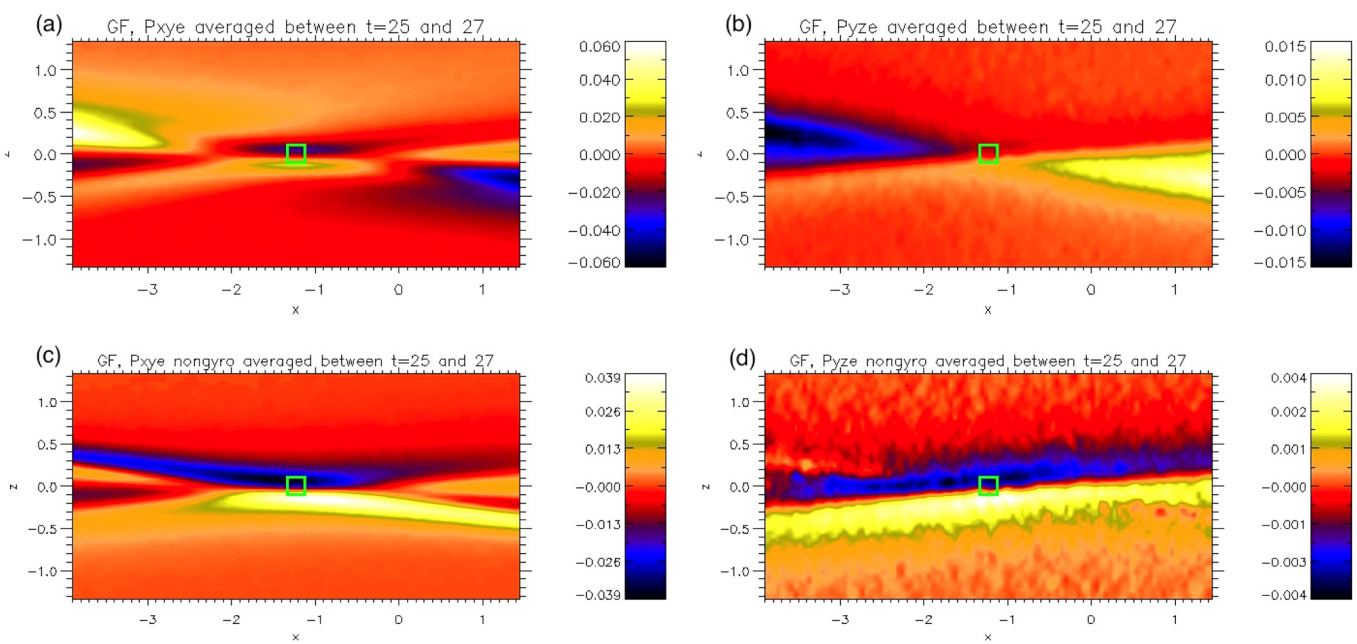

FIG. 17. Electron pressure tensor components for the Harris plus constant guide field case, for data averaged between $t = 25$ and $t = 27$. Shown are (a) P_{xye}, (b) P_{yze}, (c) $P_{xye,ng}$, (d) $P_{yze,ng}$.

This is clearly a point which should be investigated in future studies.

IV. SUMMARY AND CONCLUSIONS

In this paper, we have investigated how the reconnection process differs when adding a non-uniform guide field to the Harris sheet, instead of a constant guide field. We have presented results from a 2.5D fully electromagnetic particle-in-cell simulation of collisionless magnetic reconnection, starting from a force-free Harris sheet with added perturbation and using the exact collisionless distribution function solution from Ref. 26 to initialise the particle velocities. For comparison, we have also presented results from a Harris sheet simulation, and a Harris sheet plus uniform guide field simulation.

We have found, as expected, that as time evolves in the force-free Harris sheet simulation, there are signs of a transition from guide field to anti-parallel reconnection. First, on the macroscopic level, the initially rotated current sheet (similar to the constant guide field case) becomes more horizontally oriented (more like the Harris sheet case) as time progresses. Second, there is a gradual decrease in the guide field B_y at the dominant X-point, indicating that it becomes less important as time proceeds. Third, the transition can also be seen by looking at the ratio of the electron Larmor radius in the guide field B_y and the electron bounce width in the reconnecting field component, B_x. The effect of the guide field on the electron orbits is significant if the ratio is less than unity.[21] At the beginning of the simulation, the ratio is well below unity, and begins to increase, eventually becoming greater than unity at a time of around $t = 25$. Finally, there are signs of a transition in the structure of the off-diagonal components of the electron pressure tensor. Initially, in the force-free case, the structure and direction of the gradient in the vicinity of the X-point are more similar (qualitatively) to the constant guide field case, but at a later time in the evolution, the structure looks more similar to the Harris case. It should be noted, however, that the transition we see is not as clear as going from purely guide field reconnection to purely anti-parallel reconnection, but instead, we see initially primarily signatures of guide field reconnection and signatures of both guide field and anti-parallel reconnection as the system evolves. This may be due to the fact that while B_y at the dominant reconnection site decreases over time, it does not vanish completely, and there is a modified quadrupolar structure of B_y at later times—not a transition to the quadrupolar structure seen in Harris sheet simulations. This could cause some features of guide field reconnection to persist and is certainly a point open to further investigation.

The dominant contribution to the reconnection electric field, E_y, was found to come from gradients of the off-diagonal components of the electron pressure tensor, in agreement with previous findings for Harris and Harris plus constant guide field setups.[3,5–8,12,13,16]

In this investigation, we have used only one set of parameters for the force-free run, which corresponds to a case where the ion distribution function is single-peaked in v_y, and has a double maximum in the v_x-direction, for small values of z around zero. The electron distribution function is single-peaked in both v_x and v_y. The distribution functions can of course both be single-peaked in v_x for other sets of parameters, and can also have more pronounced double maxima in v_x, as well as a double maximum in v_y.[27] A future study could investigate how the evolution of the system depends on the initial velocity space profile for this equilibrium. The dependence of the evolution on other parameters could be investigated, such as mass ratio, temperature ratio, or initial current sheet thickness.

ACKNOWLEDGMENTS

This project has received funding from the European Union's Seventh Framework Programme for research, technological development, and demonstration under Grant Agreement No. SHOCK 284515 (F.W. and T.N.). Website: project-shock.eu/home/. We also acknowledge financial support from the Leverhulme Trust, under Grant No. F/00268/BB (C.S., F.W., and T.N.); the U.K. Science and Technology Facilities Council via consolidated Grant No. ST/K000950/1 (F.W. and T.N.) and PhD studentship Reference No. PPA/S/S/2005/04216 (M.G.H.); and NASA's Magnetospheric Multiscale Mission (M.H.).

[1]D. Biskamp, *Magnetic Reconnection in Plasmas* (Cambridge University Press, 2000).
[2]J. Birn and E. R. Priest, *Reconnection of Magnetic Fields: Magnetohydrodynamics and Collisionless Theory and Observations* (Cambridge University Press, 2007).
[3]M. M. Kuznetsova, M. Hesse, and D. Winske, J. Geophys. Res. **103**, 199, doi:10.1029/97JA02699 (1998).
[4]M. A. Shay, J. F. Drake, R. E. Denton, and D. Biskamp, J. Geophys. Res. **103**, 9165, doi:10.1029/97JA03528 (1998).
[5]M. Hesse, K. Schindler, J. Birn, and M. Kuznetsova, Phys. Plasmas **6**, 1781 (1999).
[6]M. M. Kuznetsova, M. Hesse, and D. Winske, J. Geophys. Res. **105**, 7601, doi:10.1029/1999JA900396 (2000).
[7]M. M. Kuznetsova, M. Hesse, and D. Winske, J. Geophys. Res. **106**, 3799, doi:10.1029/1999JA001003 (2001).
[8]P. L. Pritchett, J. Geophys. Res. **106**, 3783, doi:10.1029/1999JA001006 (2001).
[9]M. Hesse, J. Birn, and M. Kuznetsova, J. Geophys. Res. **106**, 3721, doi:10.1029/1999JA001002 (2001).
[10]M. Hesse, K. Schindler, M. Kuznetsova, and M. Hoshino, Geophys. Res. Lett. **29**, 1563, doi:10.1029/2001GL014714 (2002).
[11]B. N. Rogers, R. E. Denton, and J. F. Drake, J. Geophys. Res. **108**, 1111, doi:10.1029/2002JA009699 (2003).
[12]M. Hesse, M. Kuznetsova, and J. Birn, Phys. Plasmas **11**, 5387 (2004).
[13]P. Ricci, J. U. Brackbill, W. Daughton, and G. Lapenta, Phys. Plasmas **11**, 4102 (2004).
[14]P. L. Pritchett and F. V. Coroniti, J. Geophys. Res. **109**, 1220, doi:10.1029/2003JA009999 (2004).
[15]M. Hesse, M. Kuznetsova, K. Schindler, and J. Birn, Phys. Plasmas **12**, 100704 (2005).
[16]P. L. Pritchett, Phys. Plasmas **12**, 062301 (2005).
[17]M. Hesse, Phys. Plasmas **13**, 122107 (2006).
[18]W. Daughton and H. Karimabadi, Phys. Plasmas **14**, 072303 (2007).
[19]W. Wan, G. Lapenta, G. L. Delzanno, and J. Egedal, Phys. Plasmas **15**, 032903 (2008).
[20]W. Daughton, V. Roytershteyn, H. Karimabadi, L. Yin, B. J. Albright, B. Bergen, and K. J. Bowers, Nat. Phys. **7**, 539 (2011).
[21]M. Hesse, T. Neukirch, K. Schindler, M. Kuznetsova, and S. Zenitani, Space Sci. Rev. **160**, 3 (2011).
[22]J. P. Eastwood, T. D. Phan, M. Øieroset, M. A. Shay, K. Malakit, M. Swisdak, J. F. Drake, and A. Masters, Plasma Phys. Controlled Fusion **55**, 124001 (2013).
[23]M. Hesse, N. Aunai, S. Zenitani, M. Kuznetsova, and J. Birn, Phys. Plasmas **20**, 061210 (2013).

[24]N. Aunai, M. Hesse, C. Black, R. Evans, and M. Kuznetsova, Phys. Plasmas **20**, 042901 (2013).
[25]E. G. Harris, Nuovo Cimento **23**, 115 (1962).
[26]M. G. Harrison and T. Neukirch, Phys. Rev. Lett. **102**, 135003 (2009).
[27]T. Neukirch, F. Wilson, and M. G. Harrison, Phys. Plasmas **16**, 122102 (2009).
[28]N. A. Bobrova, S. V. Bulanov, J. I. Sakai, and D. Sugiyama, Phys. Plasmas **8**, 759 (2001).
[29]H. Li, K. Nishimura, D. C. Barnes, S. P. Gary, and S. A. Colgate, Phys. Plasmas **10**, 2763 (2003).
[30]K. Nishimura, S. P. Gary, H. Li, and S. A. Colgate, Phys. Plasmas **10**, 347 (2003).
[31]J.-I. Sakai and A. Matsuo, Phys. Plasmas **11**, 3251 (2004).
[32]K. Bowers and H. Li, Phys. Rev. Lett. **98**, 035002 (2007).
[33]E. Moratz and E. W. Richter, Z. Naturforsch., A **21**, 1963 (1966).
[34]A. Sestero, Phys. Fluids **10**, 193 (1967).
[35]F. Wilson and T. Neukirch, Phys. Plasmas **18**, 082108 (2011).
[36]C. R. Stark and T. Neukirch, Phys. Plasmas **19**, 012115 (2012).
[37]B. Abraham-Shrauner, Phys. Plasmas **20**, 102117 (2013).
[38]O. Allanson, T. Neukirch, F. Wilson, and S. Troscheit, Phys. Plasmas **22**, 102116 (2015).
[39]M. G. Harrison, "Equilibrium and dynamics of collisionless current sheets," Ph.D. thesis, University of St Andrews, 2009.
[40]F. Wilson, "Equilibrium and stability properties of collisionless current sheet models," Ph.D. thesis, University of St Andrews, 2013.